Article

KOH-doped Porous Polybenzimidazole Membranes for Solid Alkaline Fuel Cells

Jong-Hyeok Park and Jin-Soo Park * iD

Department of Green Chemical Engineering, College of Engineering, Sangmyung University, Cheonan 31066, Korea; sbq6358@gmail.com
* Correspondence: energy@smu.ac.kr; Tel.: +82-41-550-5315

check for updates

Abstract: In this study the preparation and properties of potassium hydroxide-doped meta-polybenzimidazole membranes with 20–30 μm thickness are reported as anion conducting polymer electrolyte for application in fuel cells. Dibutyl phthalate as porogen forms an asymmetrically porous structure of membranes along thickness direction. One side of the membranes has a dense skin layer surface with 1.5–15 μm and the other side of the membranes has a porous one. It demonstrated that ion conductivity of the potassium hydroxide-doped porous membrane with the porogen content of 47 wt.% (0.090 S cm^{-1}), is 1.4 times higher than the potassium hydroxide-doped dense membrane (0.065 S cm^{-1}). This is because the porous membrane allows 1.4 times higher potassium hydroxide uptake than dense membranes. Tensile strength and elongation studies confirm that doping by simply immersing membranes in potassium hydroxide solutions was sufficient to fill in the inner pores. The membrane-electrode assembly using the asymmetrically porous membrane with 1.4 times higher ionic conductivity than the dense non-doped polybenzimidazole (*m*PBI) membrane showed 1.25 times higher peak power density.

Keywords: polybenzimidazole; solid alkaline fuel cell; asymmetrically porous film; porogen

1. Introduction

Fuel cells are considered to be low-pollution and high-efficiency energy conversion technology which directly convert fuel energy into electricity. Proton exchange membrane fuel cells (PEMFCs) are currently used in the niche energy market due to intensive research and development of proton exchange membranes, especially perfluorinated sulfonic acid ionomers. Solid alkaline fuel cells (SAFCs) are fuel cell technology using anion exchange membranes for the conduction of hydroxide ions from cathode to anode. Much attention has been recently received due to several advantages such as enhanced oxygen reduction in an alkaline environment, less expensive membrane materials, and easier water management. The recent review paper reported very good peak power density over 1 W/cm^2 at 0.5–0.7 V for pure hydrogen as fuel and a Pt-based catalyst [1]. Nevertheless, anion exchange membranes still suffer from lower ionic conductivity than proton exchange membranes, since the electrical mobility of hydroxide ions is only 56% of that of protons In addition, the review found that the durability of most of the cells reported was limited to less than 1000 h [1]. The main reason for the poor performance stability of SAFCs is due to the chemical degradation of cationic functional groups of anion exchange membranes. Anion conductive polymers must exhibit high chemical, mechanical and thermal stability, as well as good ion conduction ability. Most of the functional groups of anion conductive polymers used are quaternized ammonium groups, which show low chemical and thermal stability due to nucleophilic displacement or Hoffman elimination in alkaline environments above 80 °C [2,3]. Hence, anion-conducting ionomers with no positively charged functional groups weak to

alkaline environments and with additional function to increase hydroxide ion conductivity are highly recommended for SAFCs [4–11].

Polybenzimidazole (PBI) shows unique amphoteric characteristic and is widely used in applications requiring excellent thermo-mechanical stability. Acid-doping (mostly phosphoric acid) PBI is commonly used in proton exchange membranes for fuel cells [12,13]. A heterocyclic benzimidazole ring with amphoteric characteristic could, however, protonate and deprotonate in acidic and basic environments, respectively. Hence, PBI can be equilibrated in aqueous solutions of alkali metal hydroxides to obtain anion conduction. In other words, (-N=) and (-NH-) of imidazole groups can be used as ion conductors by reacting with acids or bases. Potassium hydroxide (KOH)-doped PBI is used as anion conductive polymer where an alkaline solution in alkaline direct alcohol fuel cells or water electrolyzers is used as fuel. PBI satisfies the aforementioned recommendations for anion exchange membranes, such as no positively charged functional group and function of anion conduction [14–21]. However, during SAFC operations using pure hydrogen and air, the hydroxide ions doped in PBI might be reduced directly leading to a decrease in ionic conductivity. In addition, the leakage of doped hydroxide ions is inevitable due to the water generated at the anode and moved toward the cathode during the operation of SAFC [16].

In this study, asymmetrically porous PBI membranes (~30 μm) were prepared in order to obtain good hydroxide ion conductivity by containing hydroxide ions in pores along with hydroxide ions doped in PBI as well as to minimize leakage of hydroxide ions during SAFC operations by making a dense surface on one side of the asymmetrically porous membranes.

2. Materials

m-PBI (Dapazol®, MW 43 kDa) was purchased from Danish power system (DPS, Kvistgård, Denmark). N,N-dimethylacetamide (DMAc) as organic solvent and dibutyl phthalate as porogen were purchased from Sigma Aldrich Chemical Co. (St. Louis, MO, USA) and were used without further purification.

3. Experiment Methods

3.1. Preparation of Asymmetrically Porous PBI Membranes

Asymmetrically porous membranes using PBI were prepared using the following method: 2 g of PBI and 18 g of DMAc were added to a round three-necked flask and then mixed under nitrogen purging and a reflux at 120 °C for at least 12 h. Dibutyl phthalate as porogen was then added and mixed again for 3 h. The resulting mixed solution was cooled down to room temperature. The prepared mixed solution was stored for 12 h at ~3 °C and was then cast to be a layer with a thickness of 250 μm on a glass plate using a doctor blade. The coated glass plate was heated in a dry oven from 25 °C to 80 °C and then dried for 8 h at 120 °C. Finally, the solid film was completed in a vacuum for 12 h. A glass plate with a cast membrane was immersed in distilled water. The cast membrane was removed from the glass plate and immersed in methanol for 12 h and in a mixture of methanol/distilled water (1:1) for 12 h to completely remove porogen imbedded inside the membranes. The membrane was finally dried at 80 °C in a convective dry oven. Asymmetrically porous PBI membranes with various contents of porogen as summarized in Table 1 were prepared in the same manner.

3.2. Ion Conductivity and the Level of KOH Doping

The asymmetrically porous PBI membranes (P-PBI) prepared were doped by soaking in 6 M potassium hydroxide (KOH). The ionic conductivity of the KOH-doped membranes was measured at every 48-h interval in order to monitor the change in the level of doping of the membranes. The hydroxide ion conductivity of KOH-doped PBI membranes was measured in a clip cell system as illustrated in Figure 1 supplying an AC power source with a frequency range of 0.01 to 10^5 Hz and a voltage intensity of 10 mV using the potentiostat/galvanostat with a frequency response analyzer (Bio-Logics 150, Paris, France). The ion conductivity σ value of the membranes was obtained using the following formula with the impedance R value measured:

$$\sigma = \frac{t}{(R - R_{blank})A} \tag{1}$$

where σ is the hydroxide ion conductivity, t is the thickness of the membrane, R is the impedance of the polymer electrolyte membrane between two electrodes, R_{blank} is the impedance R of the KOH solution between two electrodes, and A is the surface area (cm^2) of the electrode in the clip cell [17].

Table 1. Composition for asymmetrically porous polybenzimidazole (PBI) membranes.

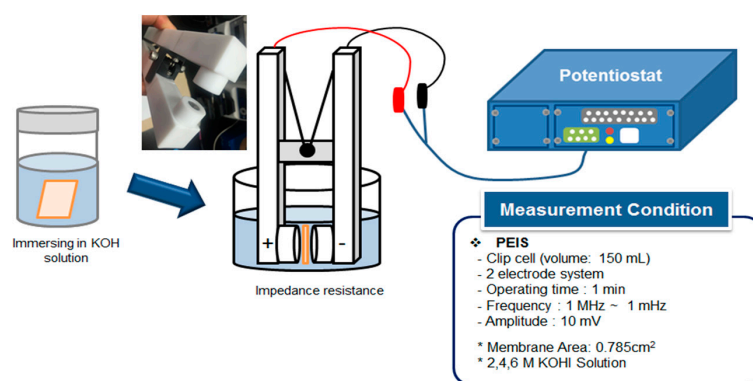| Sample Name	*m*PBI	Porogen (g)	Porogen Content (wt.%)
*m*PBI	2	0	0
P-PBI 41	2	1	41
P-PBI 44	2	1.6	44
P-PBI 47	2	1.8	47

Figure 1. Clip cell for the measurement of impedance resistance.

The level of doping of KOH was measured to evaluate the effect on the actual conductivity. The KOH impregnation amount of the membrane was calculated using the following equation:

$$\text{KOH Uptake}(\%) = \frac{W_s - W_d}{W_d} \times 100 \tag{2}$$

where, W_s and W_d represent the weight of the wet and the dry membrane, respectively.

3.3. Characterization of KOH-doped Asymmetrically Porous PBI Membranes

The surface and cross-sectional images of the asymmetrically porous PBI membranes prepared were acquired by a field emission scanning electron microscope (SEM) (ULTRA PLUS, Carl Zeiss, Oberkochen, Germany) with an electron beam of 3 kV. The membranes were dried overnight in a vacuum oven at room temperature and then coated with gold (Au) using a sputter coater (Med 010, Oerlikon Balzers, Balzers, Liechtenstein) *to* achieve a specific coating thickness (~10 nm). SEM images were analyzed in terms of pore size and distribution using the image J program. The cast membranes were analyzed using an attenuated total reflectance (ATR) unit of Fourier transform infrared (FTIR) (/Raman spectrometer (IFS 66/S, Bruker Optik GmbH, Ettlingen, Germany).

The thermal stability of KOH-doped asymmetrically porous PBI membranes was evaluated using thermogravimetric analysis (TGA) (TGA 2050 CE, TA instruments, Inc., New Castle, DE, USA) at a rate of 10 °C min^{-1} from room temperature to 800 °C under a nitrogen atmosphere.

Tensile strength tests of un- and doped membranes using a micro material tester (Model 5848, Instron, Norwood, MA, USA) were measured to evaluate mechanical stability at 5.00 mm min^{-1} at ambient temperature and humidity. The sample shape was rectangular with a width of 10 mm and a length of 30 mm. All other procedures were based on the ASTM D882 standard test method.

3.4. Fabrication and Evaluation of Membrane-Electrode Assembly

For the electrochemical analyses of the asymmetrically porous PBI membranes prepared, a membrane-electrode assembly (MEA) was prepared by gas diffusion layer electrodes (GDE) using commercially available gas diffusion layers (23BC, SIGRACET®, SGL Carbon, Wiesbaden, Germany). The electrode has the effective area of 9 cm^2 with 0.4 mg of Pt/cm^2 for each electrode. A pair of GDEs and the KOH-doped membrane were assembled with the clamping pressure of the cell of 50 kgf. The dense surface of the asymmetrically porous membranes was faced to the anode for all MEAs, unless specifically stated. MEA performance tests were performed using KOH-doped GDE prepared by immersion in 6 M KOH for 24 h on both sides of alkali-doped asymmetrically porous PBI membrane. The performance and characterization of the MEAs were compared by measuring I-V polarization curves and impedance spectroscopy for high frequency resistance (HFR). The station conditions for the performance analysis of the MEAs were set at 60 °C with 0.3 L min^{-1} of hydrogen and oxygen to the anode and cathode, respectively.

4. Results and Discussion

PBI-based polymers have high thermal stability and mechanical strength, as well as excellent chemical resistance to acids and bases. In this study, thin asymmetrically porous PBI membranes with 20~30 μm thickness were prepared and used as an anion conducting membrane by doping KOH. Figure 2 shows photographs of non-porous and asymmetrically porous PBI membranes. The thin PBI membranes (on the far left hand side in Figure 2) are transparent since they have no pores. However, all of the P-PBI membranes are opaque due to light scattering by pores inside the membranes. The different colors of the upside and downside are associated with the asymmetric structure of the membranes. One side of the membranes (upside in Figure 2) is dense, while another side of the membranes (downside in Figure 2) has a porous surface. This structural difference can be confirmed in Figure 3. Figure 3 shows SEM images of both sides of the surface of the membranes of *m*PBI and P-PBI 41, 44, and 47. The upside and downside of the membranes show dense and porous surfaces, respectively. As the content of porogen increases, the number and size of pores in the downside surface of the membranes increase. As shown in the cross-sectional images of the membranes of Figure 3, all of the upside surfaces have dense skin layers, and pores are formed beneath the skin layers. The images of the downside surface show a few tiny pores in Figure 3a, but it seems that the formation of pores inside the membranes is not clear. Thus, the porogen content of 41 wt.% could be considered as the minimum amount to start forming pores inside the membranes. Table 2 summarizes the structural properties of the P-PBI membranes. It is inferred that the membrane drying results in an asymmetrically porous structure of the P-PBI membranes, since the thickness of the skin layers of the P-PBI membranes is inversely proportional to the content of porogen.
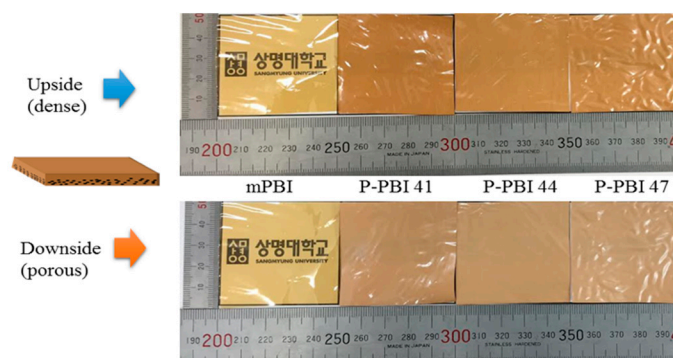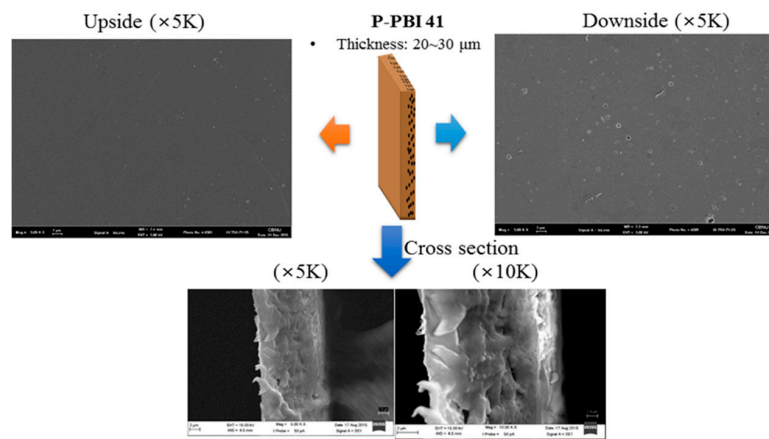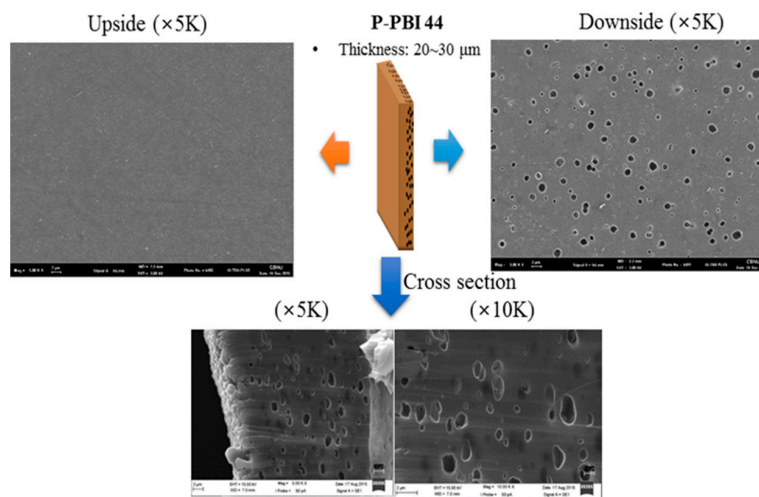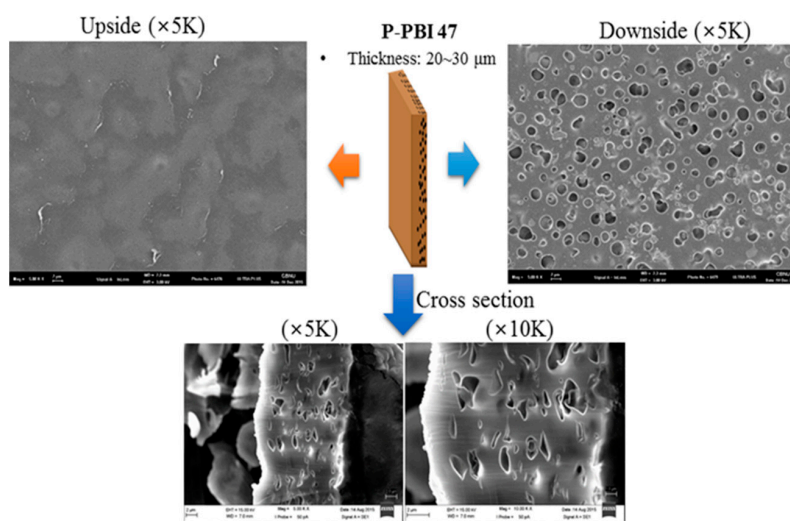

Figure 2. Photographs of non-porous and asymmetrically porous PBI membranes.

(**a**)

(**b**)

(**c**)

Figure 3. Photographs of non-porous and asymmetrically porous PBI membranes: (**a**) P-PBI 41, (**b**) P-PBI 44 and (**c**) P-PBI 47.

Table 2. Summary of the structural properties of the P-PBI membranes.

Sample Name	Average Pore Size (μm)	Range of Pore Size (μm)	Thickness of a Skin Layer
P-PBI 41	0.2	0.055–0.44	10–15
P-PBI 44	0.94	0.2–2	1.8–2
P-PBI 47	1.72	0.4–3.1	1.5

Chemical stability of the membranes in an alkaline environment during their KOH doping in a 6 M KOH solution was investigated. In Figure 4, the ATR-FTIR spectra of the KOH-doped membranes are shown, along with that of the non-doped PBI membrane (*m*PBI) as a reference. The *m*PBI membrane shows the peaks of C-N stretching at 1600 cm^{-1}, N-H at 1544 cm^{-1}, and imidazole group at 1284 cm^{-1}. After KOH doping, the adsorption peaks appear around 1625, 1510, and 1120 cm^{-1} due to the adsorption of water to O-H stretching, N-K deformation, and N-K plane bending, respectively. Compared with non-doped *m*PBI, the peak at 1284 cm^{-1} disappears and the peaks at 1510 cm^{-1} and 1120 cm^{-1} appear instead. This confirms that the group of imidazole reacts with the cation K$^+$ to contain the KOH in the membranes during KOH doping [14,17]. The P-PBI membranes show the same peaks to those of *m*PBI due to KOH doping inside polymer as well as pores.
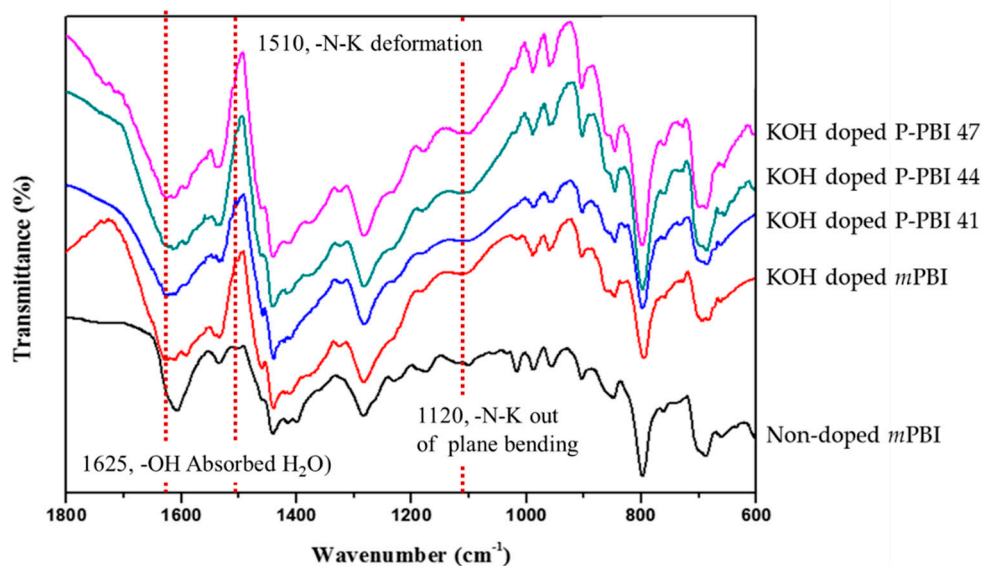
Figure 4. ATR-FTIR spectra of potassium hydroxide (KOH) doped P-PBI membranes.

The thermal and mechanical stability of the P-PBI membranes were investigated, and we tried to determine whether the porous structure weakens their mechanical properties. Figure 5 shows the TGA spectra of the non-doped and KOH-doped *m*PBI membranes and the KOH-doped P-PBI membranes. A decrease in weight up to 150 °C for all spectra is associated with dehydration of the membranes since the polybenzimidazole polymer is very hygroscopic and the KOH-doped membranes contain water absorbed during doping. No further decrease in weight up to 600 °C is shown and then the weight loss above 600 °C is associated with the decomposition of the polymer backbone [17]. The KOH-doped *m*PBI membrane shows less thermal stability than the non-doped mPBI membranes due to the plasticizing effect of KOH. Interestingly, the KOH-doped P-PBI membranes show very similar thermal stability to the KOH-doped *m*PBI membrane. This confirms that no KOH absorbed inside pores of the membranes is evaporated and no pores are collapsed up to 800 °C. Table 3 summarizes the results of the mechanical property tests on the non-doped and doped membranes to confirm the mechanical stability of the KOH-doped asymmetrically porous membranes. The non-doped membranes show much higher tensile strength than doped membranes, due to the plasticizing effect of KOH. As the content of porogen for both the non-doped and doped membranes increases, the tensile strength decreases due to

porous structure [22]. For elongation, the doped membranes obtain higher values than the non-doped membranes due to an increase in softness. The elongation of the non-doped membranes increases as the content of porogen increases. However, the elongation of the doped membranes shows the opposite trend. Pores in the non-doped membranes play a role in increasing ductility of the polymer in good agreement with the previous study [23]. However, pores in the plasticized polymer for the doped membranes show a brittle response. It might be concluded that empty pores show a response reminiscent of an elastic–plastic material to result in KOH doping which fills up pores diminishes the effect of porosity. It infers that during KOH doping by simply immersing the P-PBI membranes a KOH solution is successfully filled in pores.
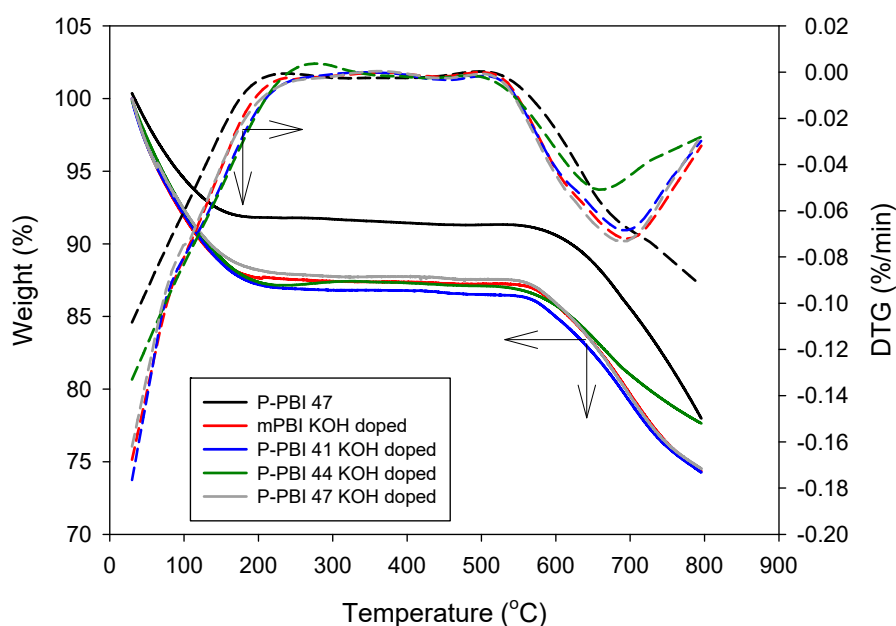

Figure 5. TGA spectra of KOH-doped P-PBI membranes.

Table 3. Properties of mechanical strength of KOH-doped *m*PBI and P-PBI membranes.

Sample Name	Non-Doped		6 M KOH-doped	
	Tensile Strength (MPa)	Elongation at Break (%)	Tensile Strength (MPa)	Elongation at Break (%)
*m*PBI	62.4 ± 1.2	6.62 ± 2.9	4.16 ± 0.65	80.6 ± 11.2
P-PBI 41	32.8 ± 2.7	8.10 ± 2.2	3.45 ± 0.46	52.9 ± 13.9
P-PBI 44	30.0 ± 0.8	10.6 ± 1.9	2.82 ± 0.34	54.3 ± 14.9
P-PBI 47	25.1 ± 2.6	11.8 ± 2.4	2.68 ± 0.54	25.8 ± 8.70

KOH doping of PBI polymer uses the reaction of (-N=) and (-NH-) with K^+ in PBI's Imidazole groups. The first mechanism is that *m*PBI, which is weakly basic due to the presence of -NH-, condenses with K^+ to generate water and hydrogen bonds. Thereafter, other excess KOH and water react with (-N=) to form an ionic bond with K^+. *m*PBI backbone is impregnated with a large amount of water, thereby forming ion clusters [24]. Figure 6 shows ion conductivity and KOH uptake of the membranes as a function of the content of porogen. Ion conductivity of the KOH-doped membranes shows a tendency to increase, even though ion conductivity of the P-PBI 44 (0.069 S cm^{-1}) slightly decreases, rather than the P-PBI 41 (0.075 S cm^{-1}), but higher than the *m*PBI (0.065 S cm^{-1}). Ion conductivity of the P-PBI 47 (0.090 S cm^{-1}) significantly increases 1.4 times higher than the *m*PBI. Nonetheless, the P-PBI 47 shows the highest ion conductivity due to surpassed KOH doping amount. This could be confirmed by KOH uptake as a function of the content of porogen. KOH uptake greatly increases as the content of porogen increases. Thus, ion conductivity should increase the similar tendency of the increase in ion

conductivity of the membranes. However, ion conductivity of the P-PBI 44 behaves in an opposite way. It can be inferred that the formation position or distribution of pores formed inside the membranes is very significant. In other words, similarly to the general phenomenon in which the well-formation of an ion cluster network (e.g., hydrophilic/hydrophobic segregation) in swelled ion conducting membranes is significant to show high ion conductivity, the P-PBI membranes might fail to have well-connected pores doped by KOH which cause lower ionic conductivity.
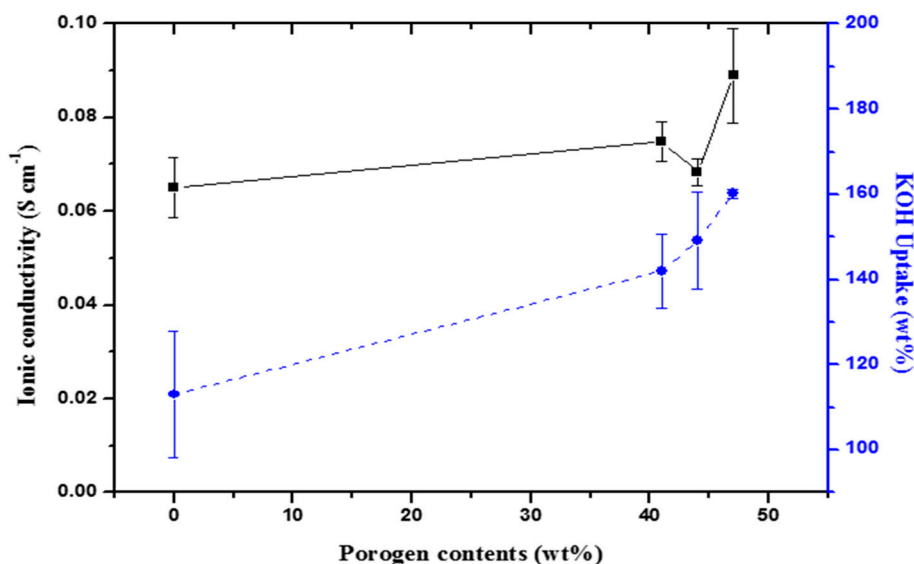

Figure 6. Ionic conductivity and KOH uptake of P-PBI membranes doped in 6 M KOH as a function of the content of porogen.

Table 4 summarizes the results of the current-voltage (I-V) polarization measurement of membrane-electrode assemblies (MEAs) using the KOH-doped membranes. Hydrogen is oxidized at the anode and oxygen is reduced at the cathode. Oxygen reduction generates hydroxide ions which migrate through the membranes towards the anode. The main two reactions are as follows:

$$\text{At anode: } H_2 + 2OH^- \rightarrow 2H_2O + 2e^-$$

$$\text{At cathode: } O_2 + 2H_2O + 4e^- \rightarrow 4OH^-$$

Open circuit voltage (OCV) of all the MEAs measured in this study exceeds 0.9 V, and thus the asymmetrically porous structure of the P-PBI membranes causes no gas crossover problem so as to prepare MEAs using the P-PBI membranes. There is no proportional relationship between the porogen content and OCV. Interestingly, the KOH-doped *m*PBI shows higher current density at high voltage (>0.55 V) than the P-PBI membranes, but the performance of the P-PBI membranes surpasses that of the *m*PBI membrane at low voltage (<0.55 V). It is associated with the characteristics of MEAs using the P-PBI membranes. The P-PBI membranes contains more KOH uptake, and KOH could be leaked out when the P-PBI membranes are compressed during unit cell assembly. Thus, KOH could fill in electrodes of MEAs to result in higher activation loss. Eventually, this affects the performance of the MEAs at voltages greater than 0.55 V. The performance of the MEAs below 0.55 V could be surpassed, since KOH filling electrodes could be ejected out of electrodes or absorbed towards the membranes, thereby resulting in decreased Ohmic loss in the MEA. In addition, the P-PBI membranes show higher ionic conductivity than the *m*PBI membranes. It is thought that the P-PBI membranes cause no serious problems in obtaining good MEA performance. Figure 7 exhibits the significantly linear relationship between the hydroxide ion conductivity of membranes and maximum power density of MEAs. It is believed that ion conductivity of membranes plays a crucial role in determining the maximum power density of MEAs. This could be a good way to increase ionic conductivity of membranes by means

of both chemical doping inside the polymer and physically contained in pores to increase the KOH uptake of the membranes. Among the P-PBI membranes, the P-PBI 44 membrane shows the lowest performance. This is due to the abnormal behavior of ionic conductivity as shown in Figure 6. The MEA using P-PBI 47_R shows similar performance at low current density and less performance at high current density. This is associated with the fact that KOH leakage from the porous surface of P-PBI 47 pronounces liquid (water generated and KOH leaked) accumulation at the anode at high current densities. Thus, this would be an advantage of asymmetrically porous membranes.

Table 4. Summary of the performance results from I-V curves of membrane-electrode assemblies using *m*PBI and P-PBI membranes.

Sample Name	OCV (V)	Current Density at 0.8 V (mA cm^{-2})	Current Density at 0.6 V (mA cm^{-2})	Current Density at 0.3 V (mA cm^{-2})	Maximum Power Density (mW cm^{-2})
*m*PBI	0.95	38.1	89.0	151	56.8
P-PBI 41	0.93	25.9	75.8	196	66.2
P-PBI 44	0.97	25.6	72.4	183	62.1
P-PBI 47	0.93	26.1	80.3	213	71.0
P-PBI 47_R *	0.94	26.4	78.2	194	65.8

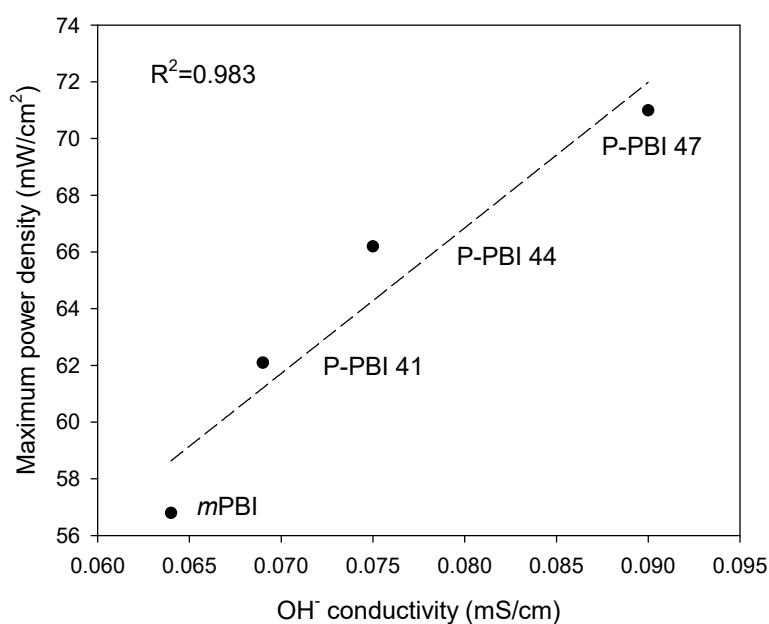* P-PBI 47_R means MEA where the dense surface of P-PBI 47 is faced to cathode.

Figure 7. Correlation of maximum power density of MEAs with hydroxide ion conductivity of membranes.

5. Conclusions

Thin asymmetrically porous PBI membranes with 20–30 μm thickness were prepared using porogen and the membranes were doped by being immersed in a 6 M KOH solution to transform PBI membranes into hydroxide ion-conducting PBI membranes. The porous PBI membranes formed asymmetrical porous structures along the thickness direction during membrane drying. Eventually, one side of the membranes has a dense surface as skin layer, having 1.5–15 out of 20–30 μm total thickness, and the other side of the membranes has a porous one. This structure allows the membranes to achieve 1.4 times higher KOH uptake and ionic conductivity than dense *m*PBI membranes. One of the asymmetrically porous membranes behaved in an opposite way, since pore distribution formed inside the membrane was not well connected. Thus, it should be considered that the content of porogen is

not only a parameter to prepare asymmetrically porous membranes with better ionic conductivity. Mechanical property measurements confirmed that KOH doping by simply immersing membranes in KOH solutions was sufficient to fill in pores. If the asymmetrically porous membranes with higher KOH uptake by chemical doping inside polymer and physical containing in pores showed higher ionic conductivity, MEAs using the membranes showed higher MEA performance. The MEA performance at high voltage (>0.55 V in this study) was worse than that of MEAs using non-porous *m*PBI membranes, due to the higher activation loss, possibly cause by leaking of KOH out of the asymmetrically porous membranes. In addition, it was found that the performance is influenced by the position of the porous surface. It is a disadvantage to apply the MEAs for residential fuel cell systems normally operated at a fixed voltage in the range of 0.7–0.75 V. To overcome this problem, in a further study, researchers could develop membranes with skin layers on both sides of the membrane and a porous structure in between skin layers to prevent KOH leaking-out and to contain higher KOH chemically and physically.

Author Contributions: Conceptualization, J.-S.P.; methodology, J.-S.P.; experimentation, J.-H.P. and J.-S.P.; validation, J.-S.P.; investigation, J.-H.P. and J.-S.P.; resources, J.-S.P.; writing—original draft preparation, J.-H.P. and J.-S.P.; writing—review and editing, J.-S.P.; supervision, J.-S.P.; project administration, J.-S.P.; funding acquisition, J.-S.P. All authors have read and agreed to the published version of the manuscript.

Conflicts of Interest: The authors declare no conflict of interest.

References

1. Dekel, D.R. Review of cell performance in anion exchange membrane fuel cells. *J. Power Sources* **2018**, *375*, 158–169. [CrossRef]
2. Tomoi, M.; Yamaguchi, K.; Ando, R.; Kantake, Y.; Aosaki, Y.; Kubota, H. Synthesis and thermal stability of novel anion exchange resins with spacer chains. *J. Appl. Polym. Sci.* **1997**, *64*, 1161–1167. [CrossRef]
3. Henkensmeier, D.; Cho, H.-R.; Kim, H.-J.; Carolina, N.-K.; Leppin, J.; Dyck, A.; Jang, J.-H.; Cho, E.; Nam, S.-W.; Lim, T.-H. Polybenzimidazolium hydroxides—Structure, stability and degradation. *Polym. Degrad. Stab.* **2012**, *97*, 264–272. [CrossRef]
4. Wang, Y.-J.; Qiac, J.; Baker, R.; Zhang, J. Alkaline polymer electrolyte membranes for fuel cell applications. *Chem. Soc. Rev.* **2013**, *42*, 5768–5787. [CrossRef]
5. Couture, G.; Alaaeddine, A.; Boschet, F.; Ameduri, B. Polymeric materials as anion-exchange membranes for alkaline fuel cells. *Prog. Polym. Sci.* **2011**, *36*, 1521–1557. [CrossRef]
6. Hickner, M.-A.; Herring, A.-M.; Coughlin, E.-B. Anion exchange membranes: Current status and moving forward. *J. Polym. Sci. Polym. Phys.* **2013**, *51*, 1727–1735. [CrossRef]
7. Maurya, S.; Shin, S.-H.; Kim, Y.; Moon, S.-H. A review on recent developments of anion exchange membranes for fuel cells and redox flow batteries. *RSC Adv.* **2015**, *5*, 37206–37230. [CrossRef]
8. Park, S.-H.; Yim, S.-D.; Yoon, Y.-G.; Lee, W.-Y.; Kim, C.-S. Performance of solid alkaline fuel cells employing anion-exchange membranes. *J. Power Sources* **2008**, *178*, 620–626. [CrossRef]
9. Park, J.-S.; Park, G.-G.; Park, S.-H.; Yoon, Y.-G.; Kim, C.-S.; Lee, W.-Y. Development of solid-state alkaline electrolytes for solid alkaline fuel cells. *Macromol. Symp.* **2007**, *249–250*, 174–182. [CrossRef]
10. Choi, J.; Byun, Y.-J.; Lee, S.Y.; Jang, J.H.; Henkensmeier, D.; Yoo, S.J.; Hong, S.-A.; Kim, H.-J.; Sung, Y.-E.; Park, J.-S. Poly(arylene ether sulfone) with tetra(quaternary ammonium) moiety in the polymer repeating unit for application in solid alkaline exchange membrane fuel cells. *Int. J. Hydrog. Energy* **2014**, *39*, 21223–21230. [CrossRef]
11. Shin, M.-S.; Byun, Y.-J.; Choi, Y.-W.; Kang, M.-S.; Park, J.-S. On-site crosslinked quaternized poly(vinyl alcohol) as ionomer binder for solid alkaline fuel cells. *Int. J. Hydrog. Energy* **2014**, *39*, 16556–16561. [CrossRef]
12. Aili, D.; Jankova, K.; Han, J.; Bjerrum, N.J.; Jensen, J.O.; Li, Q. Understanding ternary poly(potassium benzimidazolide)-based polymer electrolytes. *Polymer* **2016**, *84*, 304–310. [CrossRef]
13. Hwang, K.; Kim, J.-H.; Kim, S.-Y.; Byun, H. Preparation of polybenzimidazole-based membranes and their potential applications in the fuel cell system. *Energies* **2014**, *7*, 1721–1732. [CrossRef]

14. Couto, R.-N.; Linares, J.-J. KOH-doped polybenzimidazole for alkaline direct glycerol fuel cells. *J. Membr. Sci.* **2015**, *486*, 239–247. [CrossRef]

15. Zeng, L.; Zhao, T.-S.; An, L.; Zhao, G.; Yan, X.-H. A high-performance sandwiched-porous polybenzimidazole membrane with enhanced alkaline retention for anion exchange membrane fuel cells. *Energy Environ. Sci.* **2015**, *8*, 2768–2774. [CrossRef]

16. Hou, H.; Sun, G.; He, R.; Sun, B.; Jin, W.; Liu, H.; Xin, Q. Alkali doped polybenzimidazole membrane for alkaline direct methanol fuel cell. *Int. J. Hydrog. Energy* **2008**, *33*, 7172–7176. [CrossRef]

17. Aili, D.; Jankova, K.; Li, Q.; Bjerrum, N.-J.; Jensen, J.-O. The stability of poly (2,2′-(m-phenylene)-5,5′-bibenzimidazole) membranes in aqueous potassium hydroxide. *J. Membr. Sci.* **2015**, *492*, 422–429. [CrossRef]

18. Wang, Y.; Wang, Q.; Wan, L.; Han, Y.; Hong, Y.; Huang, L.; Yang, X.; Wang, Y.; Zaghib, K.; Zhou, Z. KOH-doped polybenzimidazole membrane for direct hydrazine fuel cell. *J. Colloid Interface Sci.* **2020**, *563*, 27–32. [CrossRef]

19. Penchev, H.; Borisov, G.; Petkucheva, E.; Ublekov, F.; Sinigersky, V.; Radev, I.; Slavcheva, E. Highly KOH doped para-polybenzimidazole anion exchange membrane and its performance in Pt/Ti_nO_{2n-1} catalyzed water electrolysis cell. *Mater. Lett.* **2018**, *221*, 128–130. [CrossRef]

20. Wu, Q.X.; Pan, Z.F.; An, L. Recent advances in alkali-doped polybenzimidazole membranes for fuel cell applications. *Renew. Sust. Energy Rev.* **2018**, *89*, 168–183. [CrossRef]

21. Konovalova, A.; Kim, H.; Kim, S.; Lim, A.; Park, H.S.; Kraglund, R.M.; Aili, D.; Jang, J.H.; Kim, H.-J.; Henkensmeier, D. Blend membranes of polybenizimidazole and an anion exchange ionomer (FAA3) for alkaline water electrolysis: Improved alkaline stability and conductivity. *J. Membr. Sci.* **2018**, *564*, 653–662. [CrossRef]

22. Zarrin, H.; Jiang, G.; Lam, G.-Y.; Fowler, M.; Chen, Z. High performance porous polybenzimidazole membrane for alkaline fuel cells. *Int. J. Hydrog. Energy* **2014**, *39*, 18405–18415. [CrossRef]

23. Yadav, S.; Saldana, C.; Murthy, T.G. Porosity and geometry control ductile to brittle deformation in indentation of porous solids. *Int. J. Solids Struct.* **2016**, *88–89*, 11–16. [CrossRef]

24. Zeng, L.; Zhao, T.-S.; An, L.; Zhao, G.; Yan, X.-H. Physicochemical properties of alkaline doped polybenzimidazole membranes for anion exchange membrane fuel cells. *J. Membr. Sci.* **2015**, *493*, 340–348. [CrossRef]